

Article

# Analysis of Suspended Particulate Matter and Its Drivers in Sahelian Ponds and Lakes by Remote Sensing (Landsat and MODIS): Gourma Region, Mali

Elodie Robert <sup>1,\*</sup>, Laurent Kergoat <sup>1</sup>, Nogmana Soumaguel <sup>2</sup>, Sébastien Merlet <sup>1</sup>, Jean-Michel Martinez <sup>1</sup>, Mamadou Diawara <sup>3</sup>  and Manuela Grippa <sup>1</sup>

<sup>1</sup> Géosciences Environnement Toulouse (CNRS, IRD, Université de Toulouse 3, CNES), 31400 Toulouse, France; laurent.kergoat@get.omp.eu (L.K.); merletsebastien1@gmail.com (S.M.); martinez@ird.fr (J.-M.M.); manuela.grippa@get.omp.eu (M.G.)

<sup>2</sup> Institute of Research for Development (IRD), BP 2528 Bamako, Mali; nogmana.soumaguel@ird.fr

<sup>3</sup> Université de Bamako, BP 2528 Bamako, Mali; diaprod@hotmail.com

\* Correspondence: elodie.robert@get.omp.eu

Received: 1 September 2017; Accepted: 29 November 2017; Published: 7 December 2017

**Abstract:** The Sahelian region is characterized by significant variations in precipitation, impacting water quantity and quality. Suspended particulate matter (SPM) dynamics has a significant impact on inland water ecology and water resource management. In-situ data in this region are scarce and, consequently, the environmental factors triggering SPM variability are yet to be understood. This study addresses these issues using remote sensing optical data. Turbidity and SPM of the Agoufou Lake in Sahelian Mali were measured from October 2014 to present, providing a large range of ‘values (SPM ranging from 106 to 4178 mg/L). These data are compared to satellite reflectance from Landsat (ETM+, OLI) and MODIS (MOD09GQ, MYD09GQ). For each of these sensors, a spectral band in the near infrared region is found to be well suited to retrieve turbidity and SPM, up to very high values ( $R^2 = 0.70$ ) seldom addressed by remote sensing studies. The satellite estimates are then employed to assess the SPM dynamics in the main lakes and ponds of the Gourma region and its links to environmental and anthropogenic factors. The main SPM seasonal peak is observed in the rainy season (June to September) in relation to precipitation and sediment transport. A second important peak occurs during the dry season, highlighting the importance of resuspension mechanisms in maintaining high values of SPM. Three different periods are observed: first, a relatively low winds period in the early dry season, when SPM decreases rapidly due to deposition; then, a period of wind-driven resuspension in January–March; and lastly, an SPM deposition period in April–May, when the monsoon replaces the winter trade wind. Overall, a significant increase of 27% in SPM values is observed between 2000 and 2016 in the Agoufou Lake. The significant spatio-temporal variability in SPM revealed by this study highlights the importance of high resolution optical sensors for continuous monitoring of water quality in these poorly instrumented regions.

**Keywords:** SPM; turbidity; surface water; remote sensing; West Africa

---

## Highlights:

- Extremely high and varying amounts of suspended particulate matter found in Sahelian ponds and lakes.
- The near infrared band is well suited to retrieve suspended particulate matter and turbidity from both MODIS and Landsat.
- An important increase in suspended particulate matter due to resuspension mechanisms is driven by wind in the dry season.

- A significant upward trend in suspended particulate matter is found for the Agoufou Lake between 2000 and 2016.

## 1. Introduction

Over the past 50 years, the Sahel has undergone significant climatic and hydrological changes. Among them, the “Sahelian paradox” refers to the observed increase in surface runoff in a context of reduced rainfall that started in the 1970s ([1–3] among others). Indeed, the Sahel drought, being the longest multi-decadal drought of the 20th century, had the unexpected consequence of more water ending up in rivers and ponds, and even in some water tables, as a result of increased preferential infiltration in ponds and gullies. The first observations of this phenomenon took place in cultivated areas of the Sahel, but, more recently, Gardelle et al. [4] and Gal et al. [5] described a spectacular increase in ponds and lakes in pastoral Sahel, in the Gourma region in northern Mali. The change was particularly important for ponds and lakes with a high turbidity and low aquatic vegetation [4]. The increase in concentrated runoff, the overall vegetation decay, and the soil erosion over shallow soils have been identified as the main factors responsible for the increase of surface water in this region [6,7]. In addition, a recent trend towards increasing daily precipitation extremes has also been detected in the Sahel [8–10]. The increase in runoff and erosion, as well as the precipitation intensification, points towards a possible increase in turbidity and suspended particulate matter (SPM) in Sahelian lakes and ponds. Beyond their importance for hydrology, sediments also impact the ecology of inland water and potentially also human health. Indeed, SPM commonly favors bacteria development and, at the same time, decreases their mortality through ultraviolet protection [11]. Some of these bacteria or microbes cause widespread water diseases like diarrhea, which is one of the major causes of mortality in children under five years in developing countries [12]. In the Gourma, like in most rural areas in the Sahel, surface water, in addition to being a fundamental resource for livestock, is largely employed for domestic activities [13,14].

Developing methods to monitor turbidity and SPM in this region, where environmental monitoring is limited, is therefore essential. In-situ information in the Sahel is scarce, hence the distribution and the dynamics of SPM in lakes and ponds (SPM level, seasonal cycles, and inter-annual variability) are poorly known.

The use of satellite data to monitor SPM and water turbidity has mainly been focused in temperate coastal areas (e.g., [15,16]), with some studies also addressing tropical areas (e.g., [17–19]) or ocean water (e.g., [20–23]). However, satellite data has proved useful to track SPM and turbidity variability in inland water in different tropical areas. Martinez et al. [24,25], for instance, used MODIS images to monitor rivers in Latin America. Feng et al. [26] also used MODIS data to study SPM dynamics in the Poyang Lake in China. In Africa, Kaba et al. [27] studied the temporal dynamics of an Ethiopian Lake using Landsat images, and Robert et al. [28] used MODIS data to document SPM and turbidity in a large reservoir in southern Burkina Faso.

These promising results suggest that a satellite survey may also be developed for the Sahel, even if remote sensing in this area may be challenging for several reasons. First, the Sahel is characterized by convective heavy rainfalls, resulting from the large squall lines of the West-African monsoon [29]. The rainy season is short, extending typically from late June to mid-September, and displays a large inter- and intra-annual variability. Vegetation growth is triggered by rainfall, but plant canopies are usually not very dense, especially in the early rainy season, so soils are prone to water erosion. All these factors favor high turbidity and SPM concentrations, and possibly also high temporal dynamics. So far, few remote sensing studies [30,31] have addressed the case of extremely turbid inland water. Second, the dry season in the Sahel is marked by very high aerosol loadings (mostly mineral dust), whereas atmospheric water vapor is very low in the dry season and very high in the monsoon season. Atmospheric corrections, which impact the quality of surface reflectance retrieval over water, may thus be challenging. All these factors may be detrimental to SPM and turbidity monitoring from space.

Due to the size of Sahelian inland waters and to the strong seasonal cycle of most ponds and lakes surface and volume [4,32,33], combining high frequency MODIS (daily) and high spatial resolution Landsat images (30 m) is particularly important to monitor water bodies in this region.

In this context, the objectives of this article are: (i) to evaluate the use of satellite data for monitoring SPM and turbidity characteristics of Sahelian water bodies; (ii) to analyze the seasonal cycle, the inter-annual variability, and the trend over 2000–present of these parameters; (iii) to investigate their spatial distribution in the Gourma region; and (iv) to investigate the links between SPM variability and climate factors (precipitation, wind), hydrological, and ecosystem variables (water height and extension in ponds and lakes, vegetation development over their watershed), as well as anthropogenic activities (livestock numbers).

## 2. Material and Methods

### 2.1. Study Area

The Gourma region is located in northern Mali, near the border with Burkina Faso (Figure 1). A long-term survey for the monitoring of vegetation and climate variables started in this area in 1984 [34]. Instrument deployment (pluviographs, meteorological, and eddy covariance fluxes) was enhanced during the AMMA (African Monsoon Multidisciplinary Analysis) campaign (2000–2010) within the frame of the AMMA-CATCH (AMMA—Coupling the Tropical Atmosphere and the Hydrological Cycle) observatory [35], and reduced thereafter due to the political instability of the region. The Agoufou Lake, which is the main target of this study, has been monitored since 2007 for water depth [5] and since 2014 for SPM and turbidity.

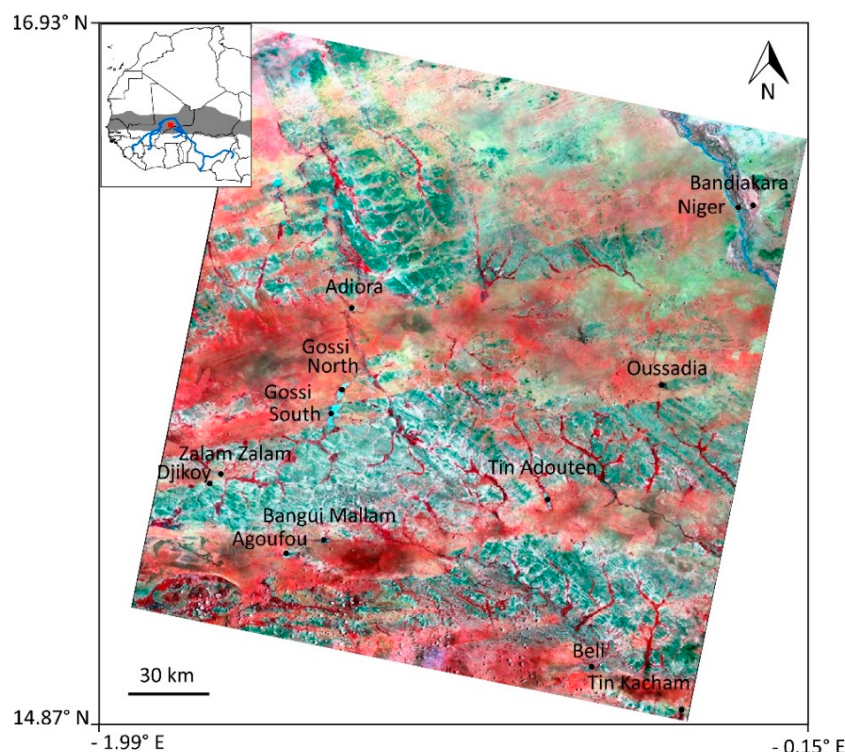


**Figure 1.** Study area. Sources: United States Geological Survey, Landsat 8 false color composite, 24 August 2013. The false color composite scheme is R = band 5 (near infrared band), G = band 4 (red band), B = band 3 (green band). The bluish color corresponds to bedrock and shallow soils on bedrock, the red color corresponds to herbaceous vegetation on deep sandy soil, and the light blue color to surface water. The gray color in the inset represents the Sahel, limited by isohyets 100 and 650 mm/year.

The climate is semi-arid, with precipitation occurring between late June and mid-September, and annual amounts ranging between 300–450 mm. Precipitation shows a high inter-annual variability: severe droughts occurred in 2004, 2008, and 2014, while positive precipitation anomalies are found for 2010, 2011 and 2013 [5].

The Agoufou Lake is the outlet of an endorheic watershed covering 183.5 km<sup>2</sup> [5], which is typical of this region where endoreism (the hydrographic network does not connect to a river) is dominant. Its size varies between about 50–70 ha at the end of dry season and 250 ha at the end of the rainy season. The Agoufou Lake, following the ecohydrological evolution of the landscape after the major droughts in the 1970s and the 1980s, changed from a seasonal to permanent regime in the 1990s [7].

Two main types of soil are found in the watershed: deep sandy soils covering the downstream portion of the watershed, on which annual herbaceous vegetation develops and some cultivation occurs, and shallow soils (silt layers or sand sheets) on bedrock (sandstones, schist, or iron pans) in the upstream part (soil map in Dardel et al. [6], Gardelle et al. [4] and Figure 15, p. 37 in Gal [36]). Livestock is the main economic activity, along with limited millet cropping occupying 5.6% of the surface in 2011 [7]. The village of Agoufou was created in the 1990s, following the change of regime of the lake.

## 2.2. In-Situ Measurements

### 2.2.1. Turbidity, SPM and Granulometry

Water samples (taken just under the surface of the water) were routinely collected every 7–10 days from October 2014 on the shore of the Agoufou Lake to perform turbidity and SPM measurements. For security reasons, the sampling was not always performed at exactly the same location (for each sample, the coordinates were recorded with a GPS). In total, 81 water samples, collected between October 2014 and October 2016, were used for this study. Twenty-four additional water samples, collected between November 2016 and October 2017, were employed to validate the relationship between SPM and satellite reflectance. Given the upper limit of the portable turbidimeter used in the field (EUTECH INSTRUMENTS Turbidimeter TN-10, 0–1000 NTU (Nephelometric Turbidity Unit), 850 nm wavelength), in-situ measurements for turbidity are not available for all the water samples collected. Some turbidity measurements, above 1000 NTU, were performed on a subsample of the collected data, with a turbidimeter ranging from 0 to 10,000 NTU (Turbidity Meter WTW TURB 555). This gives a total of 38 valid measurements for turbidity. For each sample, three measurements were made and averaged. SPM were measured by filtering the water samples using a glass microfiber filter (0.7 µm pore size). The filters were pre-weighed after being dried at 105° for 1 h 30 min and were dried again and weighed after water filtration. SPM are calculated by the difference between the dry weights after and before filtering divided by the volume of filtered water. For each sample, two measurements were made and averaged. Data pairs with at least one measurement ‘out of range’ were discarded.

Two water samples (13 September and 14 November 2014) were also analyzed for particle size distribution (PSD). The PSD was measured with a laser grain size meter Horiba LA950-V2 (Horiba Instruments, Inc., Kyoto, Japan).

### 2.2.2. Water Level

The water level of the Agoufou Lake has been monitored since 2007, every 7–10 days using a staff gauge. These data were described in detail by Gal et al. [36].

### 2.2.3. Precipitation

Daily precipitation has been measured 2 km away from the Agoufou Lake from 2003 onwards. These data have been completed by rainfall data from the Hombori SYNOP station for the years 2000, 2001, and 2002.

## 2.2.4. Wind

Wind speed and direction have been measured by an automatic weather station between 2002 and 2011 (15 min average recorded every 15 min by an anemometer—Delta T Devices AN1, and a wind wane—WD1), located 2 km away from the lake.

## 2.2.5. Livestock

Monthly livestock numbers at the Agoufou Lake have been monitored in 2010–2011. This was done by counting each herd during its passage to the watering point. Livestock numbers have been converted to Tropical Livestock Unit (TLU) based on different conversion coefficients for cattle, sheep, and goats [37,38].

## 2.3. Satellite Data

Two Landsat products were used in this study (Table 1): the Surface Reflectance (in  $\text{sr}^{-1}$ , equivalent to the remote sensing reflectance) by Landsat 7 ETM+ and by Landsat 8 OLI, available since 1999 (breakdown of a mirror in 2003) and 2013, respectively. Landsat 8 and Landsat 7 have a ground track repeat of 16 days each and a 30 m spatial resolution. The combination of the two satellites provides an acquisition every eight days (when Landsat 7 and Landsat 8 image are associated, and there are no clouds, aerosols, or stripes for Landsat 7 images), which is compatible with the field measurement sampling frequency of 7–10 days. The spatial resolution of 30 m provides interesting information on the spatial variability between several small water bodies in this region, as well as within the largest lakes. The data (path 195 row 049) were collected from the USGS (United States Geological Survey) Earth Explorer data gateway. The cloudy images, those with high levels of aerosols, and those for which the stripes in L7 masked our sampling area were removed according to the quality data (QA bands used for Landsat 7: cloud, adjacent cloud, shadow cloud, and for Landsat 8: cloud, adjacent cloud, shadow cloud, aerosol, cirrus) and after a visual check of each image.

**Table 1.** Comparison between Landsat 7 ETM+, Landsat 8 OLI, MODIS NIR, and Red spectral bands.

Spectral Band ( $\mu\text{m}$ )	Landsat-7 ETM+	Landsat-8 OLI	MODIS
Red	0.631–0.692	0.636–0.673	0.620–0.670
NIR	0.772–0.898	0.851–0.879	0.841–0.876

The Landsat time series data were supplemented with data from the daily MODIS Collection 6 reflectance products MOD09GQ (Terra on-board sensor, starting in 2000) and MYD09GQ (Aqua on-board sensor, starting in 2002), which provide calibrated surface reflectance in the red (R) and near infrared (NIR) radiometric bands at a 250 m resolution (Table 1). The daily MODIS surface reflectance products MOD09GA and MYD09GA provide information about aerosols, clouds, cloud shadows, and cirrus. The possible effect of sunglint was also calculated. Images with significant clouds, shadow cloud, cirrus, high aerosol loading, and high sunglint conditions were discarded. The MODIS data (MOD09Q1, MYD09Q1, MOD09GA, MYD09GA h7v17) acquired between March 2000 and October 2017 were downloaded through the Data Pool of the LAADS Distributed Active Archive Center (<https://ladsweb.modaps.eosdis.nasa.gov/>).

The seasonal dynamics of the vegetation over the Agoufou watershed were monitored by means of the Normalized Difference Vegetation Index (NDVI) computed from the MODIS MOD13Q1 and MYD13Q1 products (250 m and 16-days intervals). The data were obtained from the NASA Earth Data ORNL DAAC data gateway.

## 2.4. Methods

In-situ turbidity and SPM measurements were used to evaluate different indexes proposed in the literature to derive these parameters from the visible and infrared bands [25,28]. These indexes were

applied to the MODIS series (2000–2016) and Landsat 7 & 8 series (2013–2016). Only images acquired within less than two days (for MODIS) or three days (for Landsat) of the in-situ sampling dates were retained for this analysis (Table 2). The in-situ and satellite data comparison was based on one pixel only. For Landsat, the open-water pixel closest to the in-situ sampling coordinates was retained. Similarly, for the analysis of MODIS time series, among the few pixels that are always open water, the pixel closest to the sampling point was retained (it happened to always be the same pixel). Possible spatial variability within a MODIS pixel was not specifically investigated. Correlations were evaluated using the  $R^2$  (coefficient of determination, equivalent to the Pearson's correlation), significance levels ( $p \leq 0.05$ ) were calculated using the Student t-test, and temporal trends were evaluated over 2000–2016 with the R software.

**Table 2.** Number of SPM in-situ data acquired with a time difference of 0, 1, 2 and 3 days from the date of the satellite data acquisitions.

Time difference	Landsat 7 and Landsat 8 Images				MODIS Images		
	0 day	1 day	2 days	3 days	0 day	1 day	2 days
SPM	10	16	13	8	26	32	16

Different wind speed and wind direction characteristics were derived to analyze the SPM dynamics: wind speed daily average, the number of wind events (temporal frequency of 15 min) over a week, on the one hand, exceeding 8 m/s (corresponding to high wind) and, on the other hand, under 5 m/s (corresponding to calm periods), and changes in wind directions.

To analyze the spatial distribution of Landsat-derived SPM over the Gourma region, surface waters (open water only) were detected by means of a threshold on the Modified Normalized Difference Water Index (MNDWI, green band – SWIR band/Green Band + SWIR Band). Typical values found by Rokni et al. [39] for two lakes were 0.45 and 0.27. Xu [40] reported values of 0.44 for a lake and 0.56 for a river. For our study area, we applied a 0.2 threshold. The aerosol masks and the cloud masks of the Landsat reflectance products were used to discard low quality or cloudy pixels (pixels showing values of 52 and 1, respectively). These masks were not sufficient, so a threshold of 0.16 on the blue band reflectance was also considered. Moreover, in order to exclude vegetated areas, we imposed NDVI to be less than 0.2 (NDVI threshold used based on a previous study on the classification of water by Gardelle et al. [4]). We mainly focused on ponds and lakes, but a portion of the Niger River, present in the Landsat image, was also analyzed in order to check the radiometric quality.

### 3. Results

#### 3.1. Relationship between In-Situ Data and Satellite Data

Turbidity and SPM of the Agoufou Lake are characterized by significant temporal variability and extremely high values, rarely reported so far for inland waters, if mountainous areas and “gray water” (any domestic wastewater produced, excluding sewage) are excluded. In-situ SPM values range from 106 mg/L to 4178 mg/L and turbidity from 124 NTU to 3314 NTU.

The two measurements of PSD reveal the presence of very fine particles, with a main mode around 1  $\mu\text{m}$  and median values around 1.6  $\mu\text{m}$ , without significant differences between the two measurements (although a second mode appears at 10  $\mu\text{m}$  for the November sample).

In-situ coincident measurements of SPM and turbidity indicate a significant linear correlation between these two variables (Figure 2).

In-situ SPM values acquired within two to three days from the satellite acquisition (Table 2) were first regressed against different combinations of visible and infrared bands using power laws, as done in Robert et al. (2016), for MODIS and Landsat data separately. For both sensors, the best relationships are observed with the NIR band alone and with the sum of the NIR and red bands (Table 3).

The regression curves obtained using MODIS and Landsat are very close. When MODIS and Landsat data are pooled together, the best relationship ( $R^2 = 0.70$ ) is observed for the NIR band (Figure 3a,b).

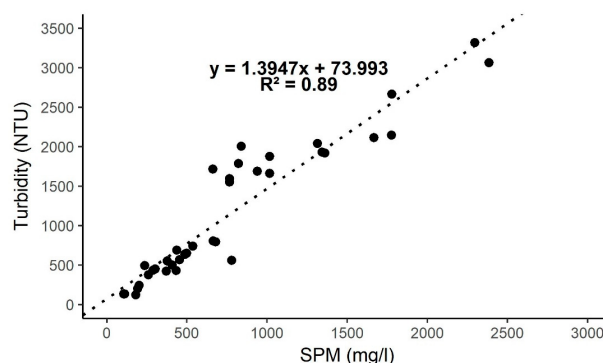


**Figure 2.** Turbidity as a function of SPM from in-situ coincident measurements over the Agoufou Lake ( $N = 38$ ).  $R^2$  indicates the Pearson's correlation.

**Table 3.**  $R^2$  for NIR bands and for the sum of the NIR and red bands as a function of SPM.  $R^2$  indicates the Pearson's correlation.

Band	$R^2$ : Landsat 7 Data vs. SPM	$R^2$ : Landsat 8 Data vs. SPM	$R^2$ : Landsat 7 and Landsat 8 Data vs. SPM	$R^2$ : MODIS Data vs. SPM	$R^2$ : MODIS and Landsat Data vs. SPM
NIR	0.42	0.83	0.73	0.68	0.70
NIR + R	0.44	0.84	0.76	0.64	0.67

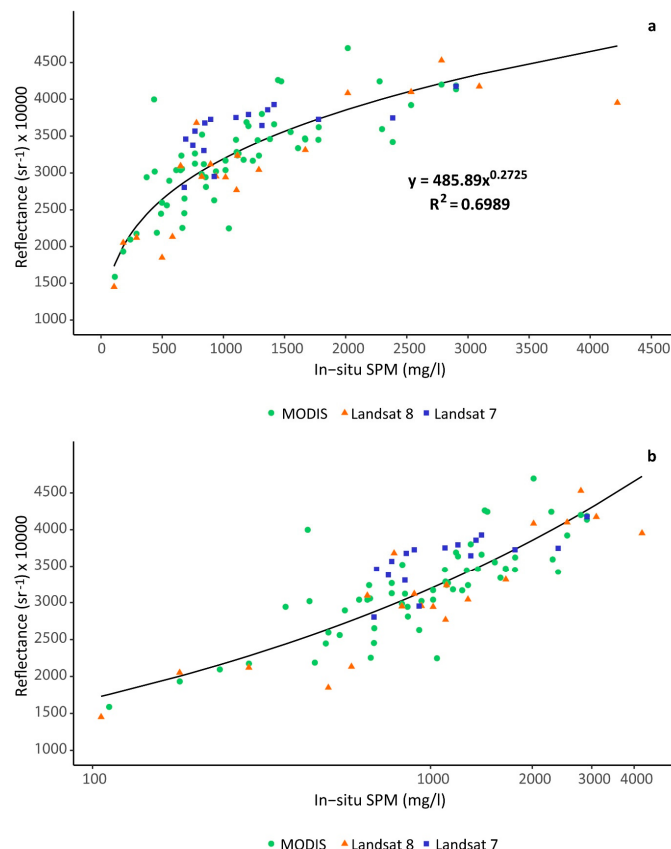


**Figure 3.** Daily MODIS and Landsat 7 and 8 NIR bands as a function of SPM in (a) linear and (b) log  $x$ -axis scale ( $N = 60$  for MODIS data and  $N = 37$  for Landsat data).  $R^2$  indicates the Pearson's correlation.

The NIR vs. SPM relation is not linear and tends to saturate at high SPM values but, overall, the NIR reflectance can be used to derive SPM up to 2500 mg/L (Figure 3). For coincident satellite acquisitions, Landsat 7 gives higher reflectance values than Landsat 8 and MODIS. Only Landsat 8 and MODIS data are therefore retained for the analysis.

The relationship between NIR reflectance and SPM was validated using an independent set of SPM measurements, acquired between November 2016 and October 2017, ranging from 570 mg/L to 2597 mg/l. SPM derived values from MODIS and Landsat 8 are well correlated to in-situ SPM ( $R^2 = 0.79$ ), with a very low bias and RMSE equal to 290 mg/L (Figure 4).

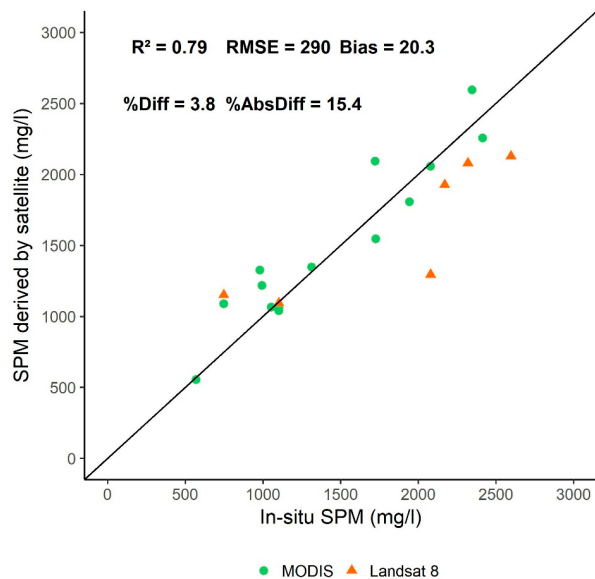


**Figure 4.** SPM derived from MODIS and Landsat vs. in-situ SPM dedicated to the validation ( $N = 14$  for MODIS data and  $N = 6$  for Landsat 8 data).  $R^2$  indicates the Pearson's correlation, RMSE the Root Mean Square Difference, bias the mean difference, %Diff the unbiased percentage difference, and %AbsDiff the absolute percentage difference. The 1:1 line is also indicated in black.

### 3.2. Seasonal and Interannual Dynamics

In all the analyses presented below, SPM concentrations are derived using the relationship obtained by regressing the NIR reflectance of MODIS and Landsat combined vs. SPM (Figure 3).

The strong seasonal dynamics observed in the in-situ data are also clearly shown by the satellite-derived SPM, either with MODIS or Landsat data (Figure 5 top). SPM displays a marked intra-annual variability, typically ranging from about 10 mg/L at the end of April to over 3000 mg/L in August. The SPM annual variability is largely related to precipitation (Figure 5 bottom). A linear regression analysis reveals that SPM is significantly correlated to the amount of rainfall cumulated over the previous seven days ( $R^2 = 0.32$ ,  $N = 2211$  for MODIS-derived SPM,  $R^2 = 0.16$ ,  $N = 81$  for in-situ SPM). The correlation is partly driven by the seasonal cycle since SPM is usually lower during the dry season. A correlation still exists when the zero-rainfall weeks are excluded ( $R^2 = 0.21$ ,  $N = 521$ ), mainly caused by precipitation between 0 and 40 mm/week (not shown). This becomes insignificant for in-situ SPM ( $R^2 = 0.06$ ,  $N = 20$ ), probably because of the low number of in-situ data during the rainy season. The first increase in SPM corresponds to the onset of the rainy season in June and SPM reaches a maximum in the core of the rainy season, between the end of July and the middle of August. This peak also roughly corresponds to the peak in water height (Figure 5) but tends to occur and end slightly earlier, with SPM starting to decrease before the end of the rainy season. The early dry season is characterized by a decrease in SPM, during which particles are deposited at the bottom of the lake. Two scenarios characterize the rest of the dry season: either a continuous decrease in SPM until June,

like in 2015 for instance, or an increase in SPM occurring between the end of January and the end of March, followed by a short decrease in May–June, like in 2013, 2014, and 2016. It is worth noting that the dry season of early 2015 follows a particularly poor 2014 rainy season, as shown in Figure 5, while the other three dry seasons (early 2013, 2014 and 2016) follow normal or above-normal rainy seasons.

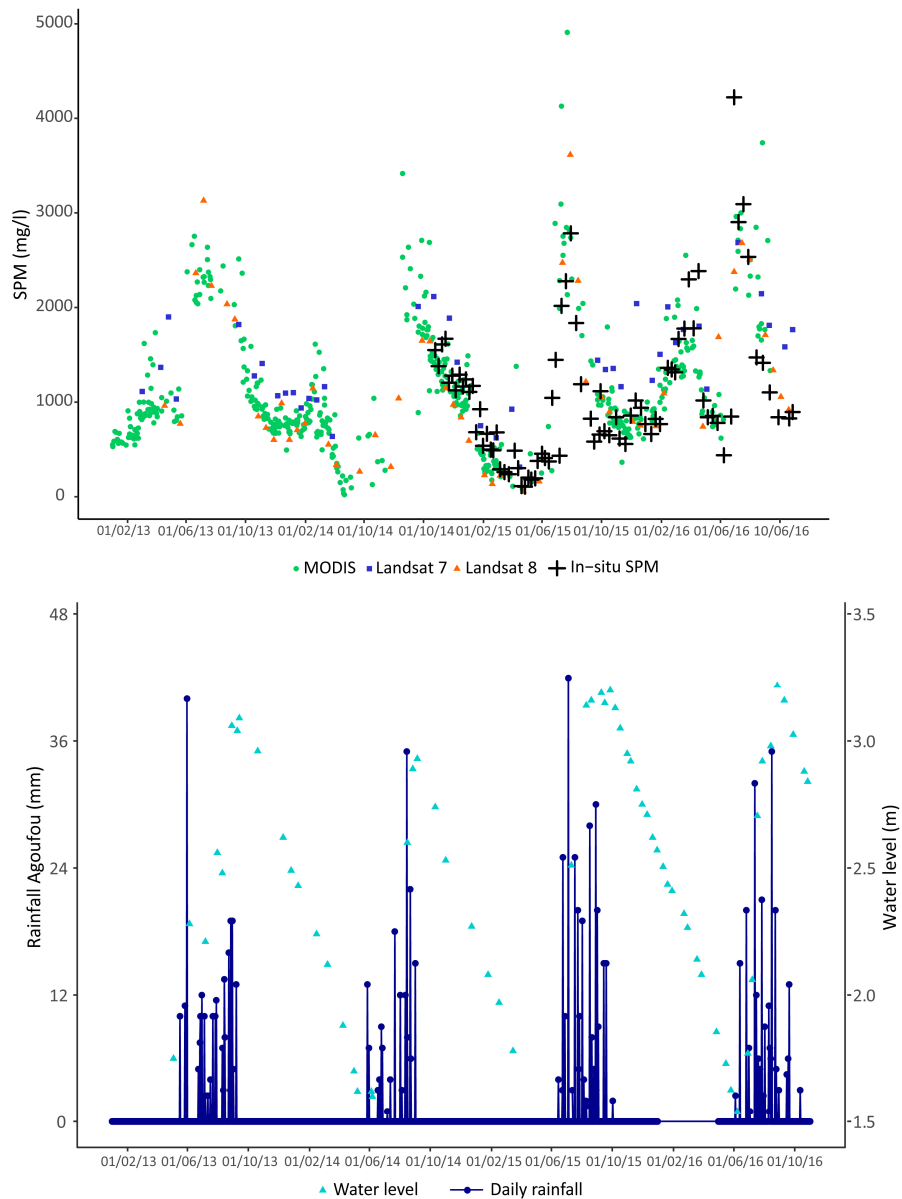


**Figure 5.** Top: SPM time series derived from MODIS, Landsat 7 and Landsat 8, and in-situ SPM. Bottom: time series of precipitation (Agoufou raingauge), and in-situ water level of the Agoufou Lake.

### 3.3. Impact of Meteorological, Hydrological and Anthropogenic Factors on the SPM Variability

To further investigate the SPM seasonal cycle, we computed seasonal averages from daily MODIS data (without clouds, aerosols, and sunglint) for the entire 2000–2016 period (see Figure 10) and for the three driest (2004, 2008, and 2014) and the three wettest (2003, 2011 and 2012, see Figure 6) years, from which average ‘dry year’ and ‘wet year’ values were computed (weekly averages were computed, and then the multi-year mean for the three driest years, the three wettest years, and all years were calculated). MODIS-derived SPM for the average dry year (Figure 6) mirrors what was found with in-situ SPM for 2014, namely a continuous decrease between August and May. Conversely, the average

'wet year' and the average over 2000–2016 ('normal year') display a marked increase of SPM from February to April, similar to that shown by in-situ data in 2016.

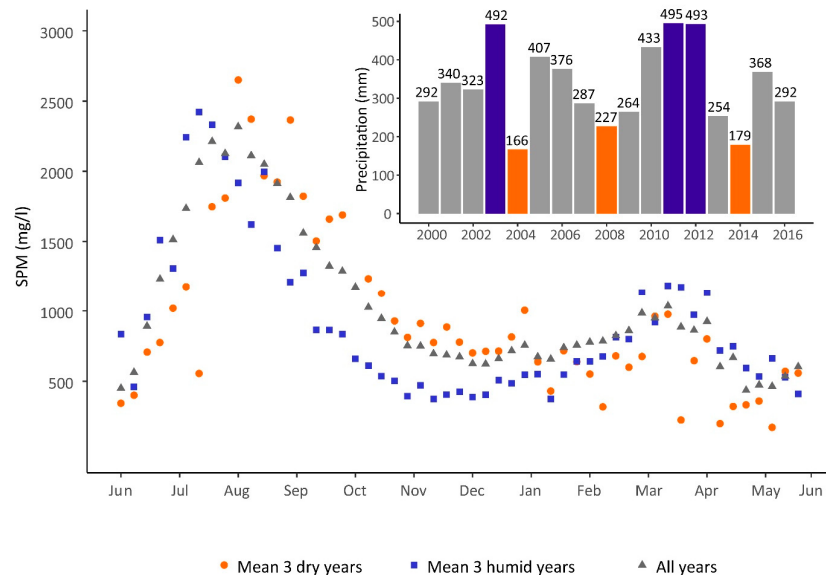


**Figure 6.** SPM seasonal cycle derived from MODIS for the Agoufou Lake: average for all years between 2000 and 2016 (gray), the three years with the lowest annual rainfall (orange), and the three years with the highest annual rainfall (blue). Annual rainfalls are shown in the inset.

Concerning the rainy season, from the third week of August onwards (i.e., in the core of the wet season), the dry year average displays higher SPM values than the normal and wet year averages, a pattern which persists during the first three months of the dry season, until the end of December.

### 3.3.1. Factors Impacting Dry Season SPM Variability

The marked dry season SPM peak, occurring for all years but the driest, could be due to different factors potentially causing particle remobilization between mid-February and mid-April and deposition afterwards, as follows:

- Particle resuspension caused by livestock gathering around and in the lake during the dry season.
- Seasonal variations in wind speed, favoring particle remobilization between mid-February and mid-April: sustained high winds are required for particle resuspension, whereas calm winds facilitate particle deposition. Wind direction may also play a role.
- Dust deposition at the lake surface.
- Variations in fetch and wave formation, caused by varying lake surface, and variation in lake depth, facilitating wave-driven friction at the lake bottom and particle resuspension [41,42].

In the following, we examine whether these factors are consistent with the temporal variations of SPM. Livestock numbers at the Agoufou Lake were extensively monitored in 2010–2011 (Figure 7), which can be considered a normal year in terms of rainfall (see bar chart in Figure 6: annual precipitation is equal to 433 mm in 2010, which falls into the group of normal years). The stocking rate around the lake increases throughout the entire the dry season, and even more so in the late dry season (May–June). This is consistent with the fact that livestock congregate around the few permanent lakes, which includes Agoufou, when other lakes or ponds have dried up. Since SPM decreases between mid-April and mid-June, livestock cannot be considered as the major driver of particle resuspension for the Agoufou Lake. In addition, livestock use the Agoufou Lake every year, which is not consistent with resuspension not occurring in the driest years.

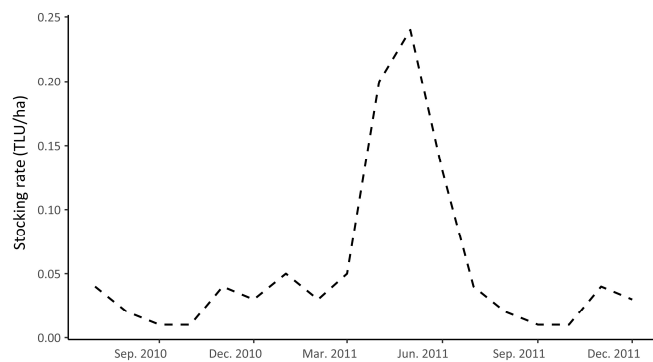


**Figure 7.** Evolution of livestock at the Agoufou Lake.

Wind speed seasonal variations are consistent with the rapid decrease of SPM after the rainy season: October-January corresponds to a period of relatively low wind speed (Figure 8), with few episodes of winds above 8 m/s (purple symbols in Figure 8) and dominant periods of wind less than 5 m/s (green symbols in Figure 8). Such calm periods favor particle deposition. Wind speed is higher in January-March, which is consistent with particle resuspension. The slight increase in the number of events with a low wind speed, at the beginning of April, could be at least partly responsible for the decrease in SPM noted for that period.

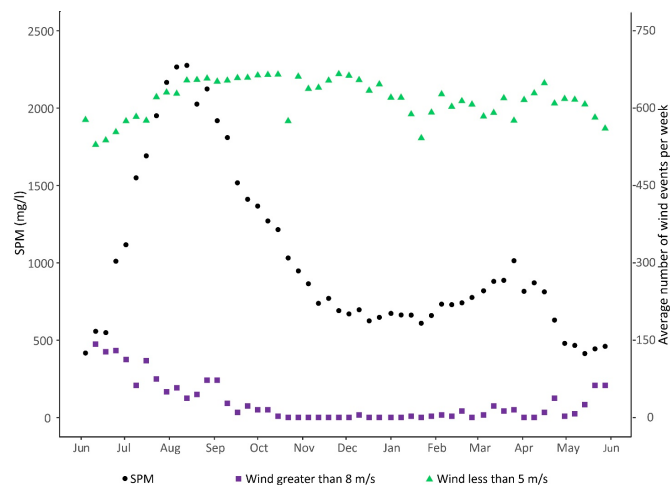


**Figure 8.** SPM mean annual cycle (average per week, 2000–2016) derived from MODIS data for the Agoufou Lake. Average number of wind events per week with a speed lower than 5 m/s and wind events with a speed greater than 8 m/s ( $\times 10$ ) for the Agoufou station, AMMA-CATCH Observatory, 2003–2010 period.

A change in wind direction is known to favor or prevent particle remobilization [43]. The Sahel experiences two main wind regimes, either the northern hemisphere trade winds, referred to as Harmattan, which blow during the dry season (mainly from East-North-East to West-South-West), or the monsoon flow, which blows during the rainy season (from South-West to North-East, Guichard et al. [44]). The transition period in Agoufou happens in April, a month during which the Intertropical Discontinuity (ITD) goes back and forth and the monsoon flow establishes with usually one or two preliminary bursts. The transition back to the Harmattan regime occurs in late October/early November. Even if this autumn transition does not seem to impact the SPM concentration (Figure 8), it cannot be excluded that the establishment of the monsoon flow in May plays a role in the decrease of SPM observed for this period.

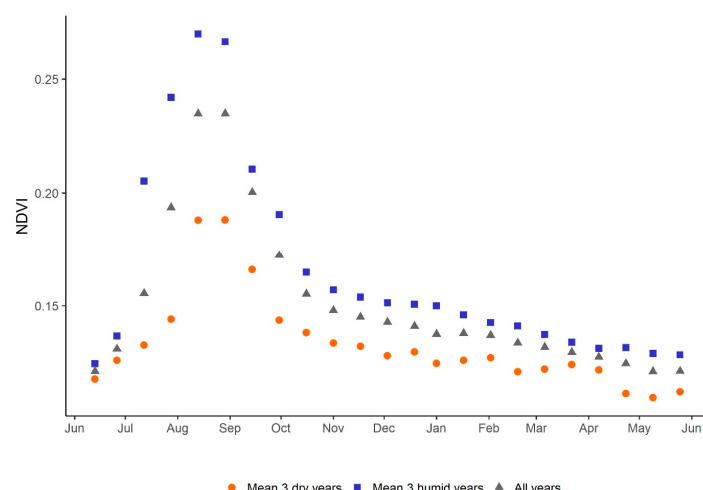
Dry and wet dust deposition may contribute to SPM in winter, spring, and summer, and less so in autumn. Sterk [45] quotes dust deposition values of 0.5 to 1.2 Mg/ha for the Harmattan season, which would correspond to an additional 50 mg/L when diluted in a 2 m water column. Dust deposition, therefore, is not important enough to impact SPM.

Figure 5 shows that during the normal years (2013–2014 and 2015–2016), the water level in the Agoufou Lake is less than 2 m from April onwards, while for the dry year (2014–2015), this level is reached as early as February. Considering that resuspension does not occur in dry years and that it stops in April–May, it is legitimate to include water depth as a possible limiting factor of SPM resuspension. Indeed, the resuspension of lake bottom sediment occurs when the water is not too deep (otherwise, the wave-driven turbulence would not reach the lake bottom), which is never the case for ponds in this region, nor too shallow (otherwise, large waves cannot develop) [46].

To summarize, dry season SPM dynamics are influenced by calm periods in the early dry season (deposition of particles in October–December), wind driven resuspension in January–March, with a possible role for low water depth inhibiting this process, and deposition again in April–May, during which the monsoon flow regime replaces the Harmattan.

### 3.3.2. Factors Impacting Rainy Season SPM Variability

The most important feature of SPM dynamics during the rainy season (Figure 8) is the sharp increase due to particles entering the lake, following the important water erosion on the watershed [7]. This pattern is commonly found in water bodies fed by surface runoff in the Sahel and is related to the high intensities of convection rainfall in this area [8], the rather low vegetation cover, and the presence of erodible material [7]. The comparison of dry, normal, and wet years, however, reveals another pattern: SPM peaks are higher and occur later in dry years. Two factors potentially contribute to this effect: Vegetation cover during dry years is markedly lower than during average or wet years (Figure 9), as it has been largely documented for the Sahel (e.g., Dardel et al. [6,47] and references therein). A lower protection of soils during dry years, and a protection occurring later, is therefore consistent with a higher SPM peak that occurs later in the rainy season and higher SPM values persisting in the early dry season. The fact that drier rainy seasons are made of a smaller number of convection events [8] is also consistent with a delay in SPM increase (due to fewer probabilities of having several large rainfall events in the early rainy season for these years). The marked decrease in SPM, starting at the core of the rainy season for wet years, may involve a limitation in material supplied to water erosion. For instance, soil particles displaced by wind erosion during the previous dry season may be rapidly washed out by the first large rainfall events.



**Figure 9.** Average NDVI cycle (2000–2016) of the Agoufou watershed from MODIS vegetation indices MOD13Q1 and MYD13Q1 (250 m and 16-days intervals) for normal, wet, and dry years.

### 3.4. Trends over 2000–2016

The analysis of the whole MODIS time series reveals a significant increase of SPM over the 2000–2016 period (Figure 10). The overall trend is equal to 27%, which corresponds to an increase of SPM from 845 mg/L to 1072 mg/L ( $p$ -value:  $1.2 \times 10^{-7}$ ). It is caused by an increase in the NIR reflectance, which is higher than the calibration drift identified for MODIS collection 6 [48]. At the monthly timescale, three months show significant trends: April, May, and July. Such a trend is consistent with the long term trend in surface runoff observed over the Agoufou watershed by Gal et al. [36], which has resulted in an increase in the lake volume over 1954–2015. A general increase in turbid water surface was diagnosed in the Gourma over 1975–2002 by Gardelle et al. [4], but the SPM trend in these turbid lakes was not documented.

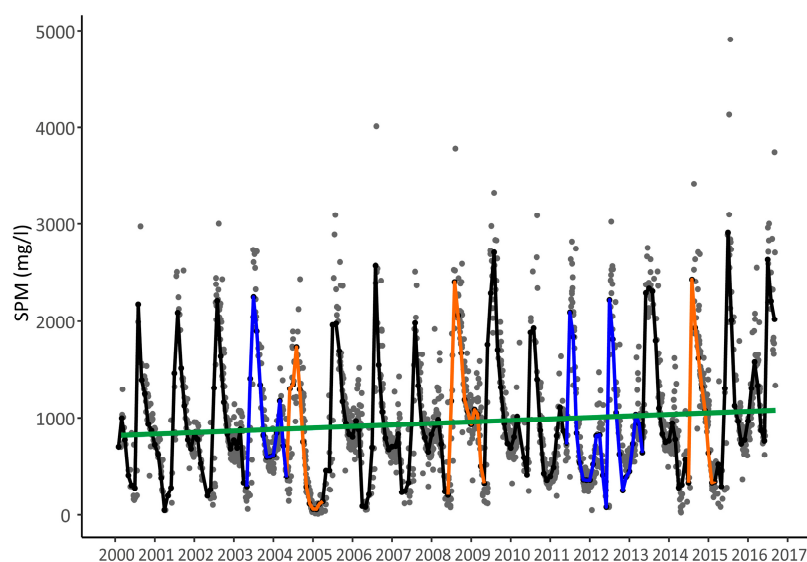


**Figure 10.** SPM time series (gray dots), monthly means (black for normal years, orange for the three driest years, and blue for the three wettest years) derived from MODIS daily data, and the trend over the 2000–2016 period (green).

The last two decades have seen the emergence of another factor that may also impact SPM, namely an intensification of the precipitation regime, suggested by Frappart et al. [8], established by Panthou et al. [9], and generalized by Taylor et al. [10]. This last study showed a threefold increase in the frequency of extreme rainfall over the last 35 years, due to a constant increase in the most intense Mesoscale Convection Systems in the Sahel and in the associated daily rainfall extremes.

### 3.5. Spatial Variability within and across Ponds and Lakes in the Gourma Region

#### 3.5.1. SPM Seasonal Cycle of Quasi Permanent Water Bodies in the Region

The seasonal cycle of SPM of all permanent or quasi-permanent lakes and water bodies in the Landsat scene was assessed for the 2013–2016 period. An example is shown in Figure 11 for the period April 2013–April 2014, which belongs to the ‘normal’ years category (Figure 6).

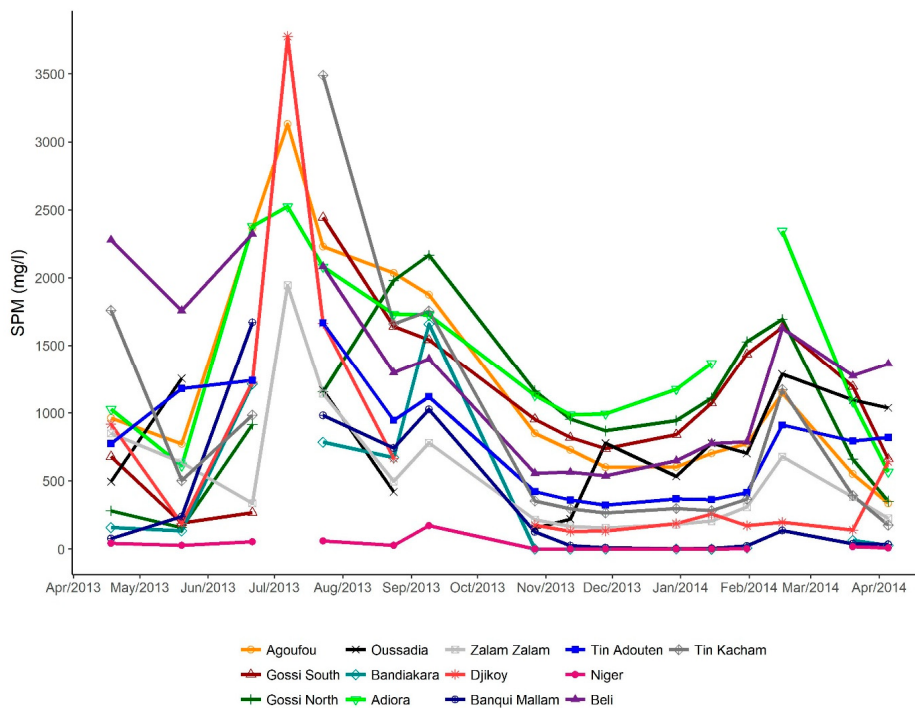


**Figure 11.** SPM seasonal cycle from Landsat 8 data for quasi-permanent water bodies in the Gourma Region (2013–2014).

Ten out of 13 water bodies exhibit a temporal variability of SPM that is similar to what is found for the Agoufou Lake. A first increase is observed from late May to early July, with a small time lag for Gossi South and Adiora (peak in late July) and a longer lag for Gossi North (peak in September). These Gossi and Adiora Lakes belong to the same valley system and SPM, being largely transported from upstream lakes, and peak later in downstream lakes. The first peak is followed by SPM decay until December–January, and by a secondary peak in February–March, with a final decay in April–May. Interestingly, the highest SPM values found in this study (the Gossi-Adiora system) correspond to the area where Gardelle et al. [4] found the highest increase in the surface area of lakes.

Overall, the SPM cycle for these 10 water bodies mirrors the SPM cycle of the Agoufou Lake, with presumably the same processes controlling SPM variability: rainy season particle inflow, early dry season deposition, wind-driven resuspension in the core of the dry season, and a final deposition linked to a combination of wind regime changes and water level/wind fetch. As the ponds differ in size, the importance of the fetch limitation in April–May is unlikely for the larger lakes like Gossi. Two ponds do not match Agoufou in terms of the seasonal SPM cycle (Djikoy and Bandiakara) and display a unimodal cycle of SPM. The fact that these are the smallest and shallowest ponds among those analyzed seems to support the idea that water depth plays a role in limiting water resuspension, which, in this case, never occurs. Finally, the Niger River shows a different behavior, which is due to its different hydrological cycle, since most of the water comes from a very distant region, after having transited through the large inner delta where most sediments are deposited. The fact that the dry season increase is not occurring in all water bodies (small ponds and Niger River) also excludes dust deposition as a major driver.

The seasonal maximum in satellite-derived SPM is above 1000 mg/L for all the lakes and ponds investigated and it is reached during the rainy season peak. The seasonal minimum in SPM values ranges from 10 mg/L (Banqui Mallam, Bandiakara) to more than 500 m/L (Agoufou, Gossi North and South, Adiora). The SPM cycle for the Beli stream (190 m wide) is similar to the SPM cycle for ponds and lakes, with relatively high values (537–2323 mg/L), as opposed to the Niger River, for which

SPM varies between 0 and 59 mg/L. Indeed, the Beli stream depends on local Sahelian hydrology, as opposed to the Niger River.

### 3.5.2. Spatial Distribution within Lakes

SPM values show a significant variability within the largest lakes (Figures 12 and 13). This is particularly evident at the beginning of the rainy season, when particles supplied by inflow generate gradients. The transport of these particles inside the lakes is particularly noticeable for Gossi (Figures 11 and 13), showing a significant lag in the time at which the SPM peak is reached between Gossi South (July) and Gossi North (September). This transfer time is classically observed for lakes [28,49,50]. The Agoufou Lake (Figure 12) sometimes shows a marked difference in sediment amount on the two sides of the road crossing it, despite the fact that water can circulate below the bridge. Resuspension during the dry season is also not uniform in space, with differences between Agoufou West and East, as well as Gossi North and South. Besides, higher SPM values are occasionally found nearby the shores.

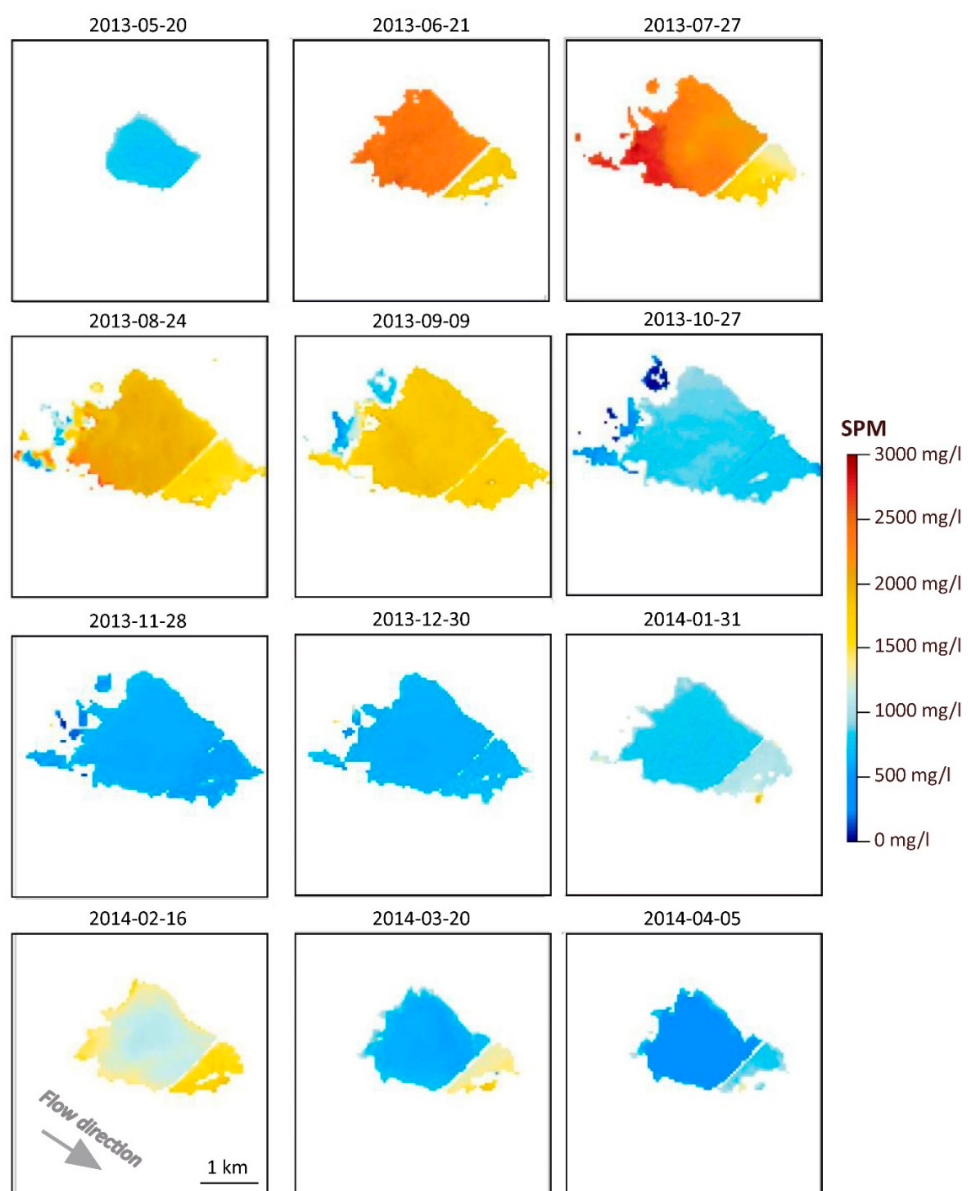


**Figure 12.** Spatial variability within the Agoufou Lake during 2013–2014.

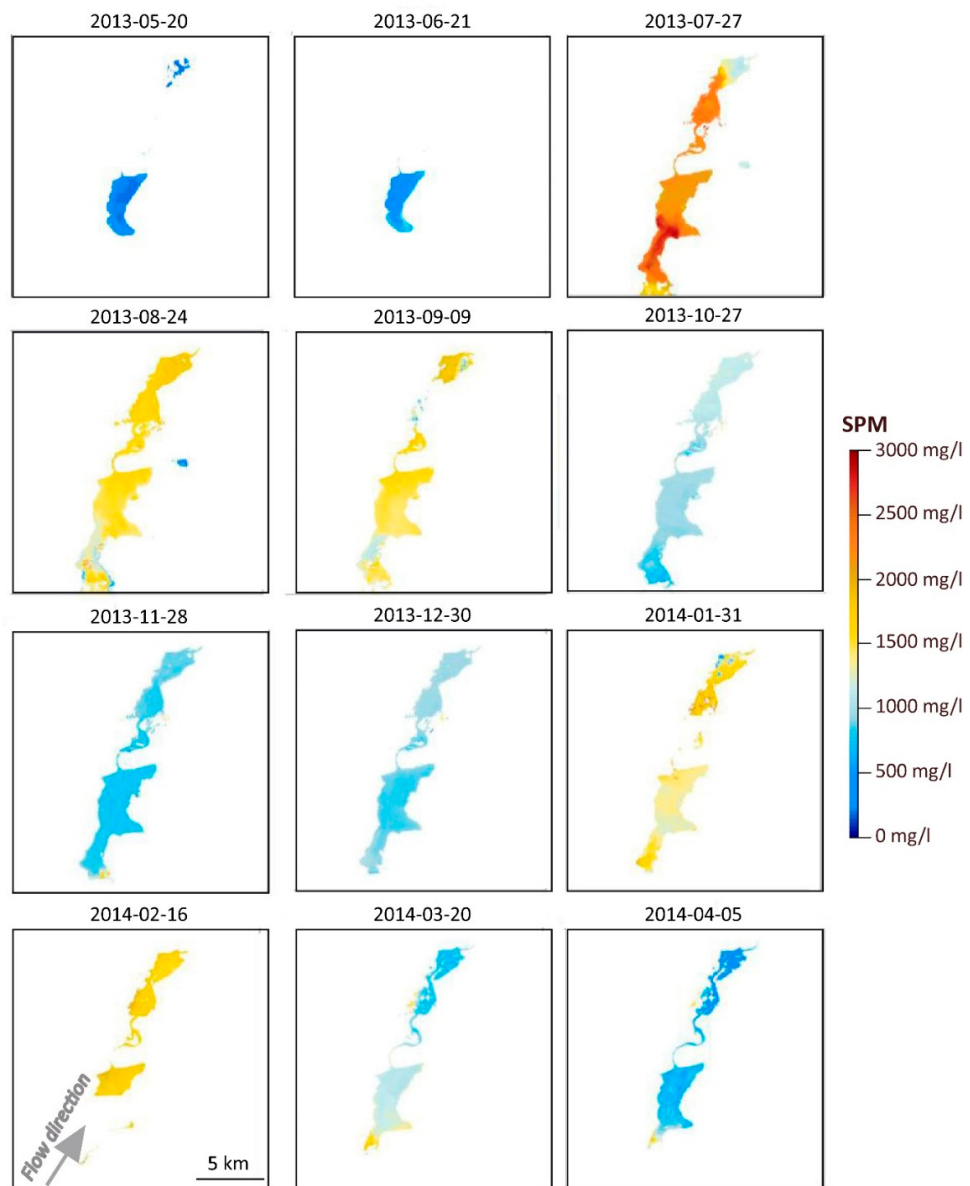


**Figure 13.** Spatial variability within the Gossi Lake during 2013–2014.

### 3.5.3. Spatial Variability across Water Bodies in the Region

Figure 14 displays the high rainy season SPM values derived from the Landsat 8 image of 24 August 2013, together with a histogram of all open water pixels. The first mode of this histogram corresponds to SPM values lower than 100 mg/L, which are located in the Niger River and, as mentioned previously, do not represent Sahelian waters. Apart from the Niger River pixels, the distribution of SPM is fairly regular, with a large mode between 600 mg/L and 1100 mg/L, a narrow mode around 1700 mg/L, and a relatively long tail extending towards large values up to 3000 mg/L. The mode at 1700 mg/L corresponds to the lakes found in the center of the Landsat scene, in the Gossi/Adiora valley system, which is fed by surface runoff from the largest area of shallow soils of this region (bluish-whitish color in Figure 1).

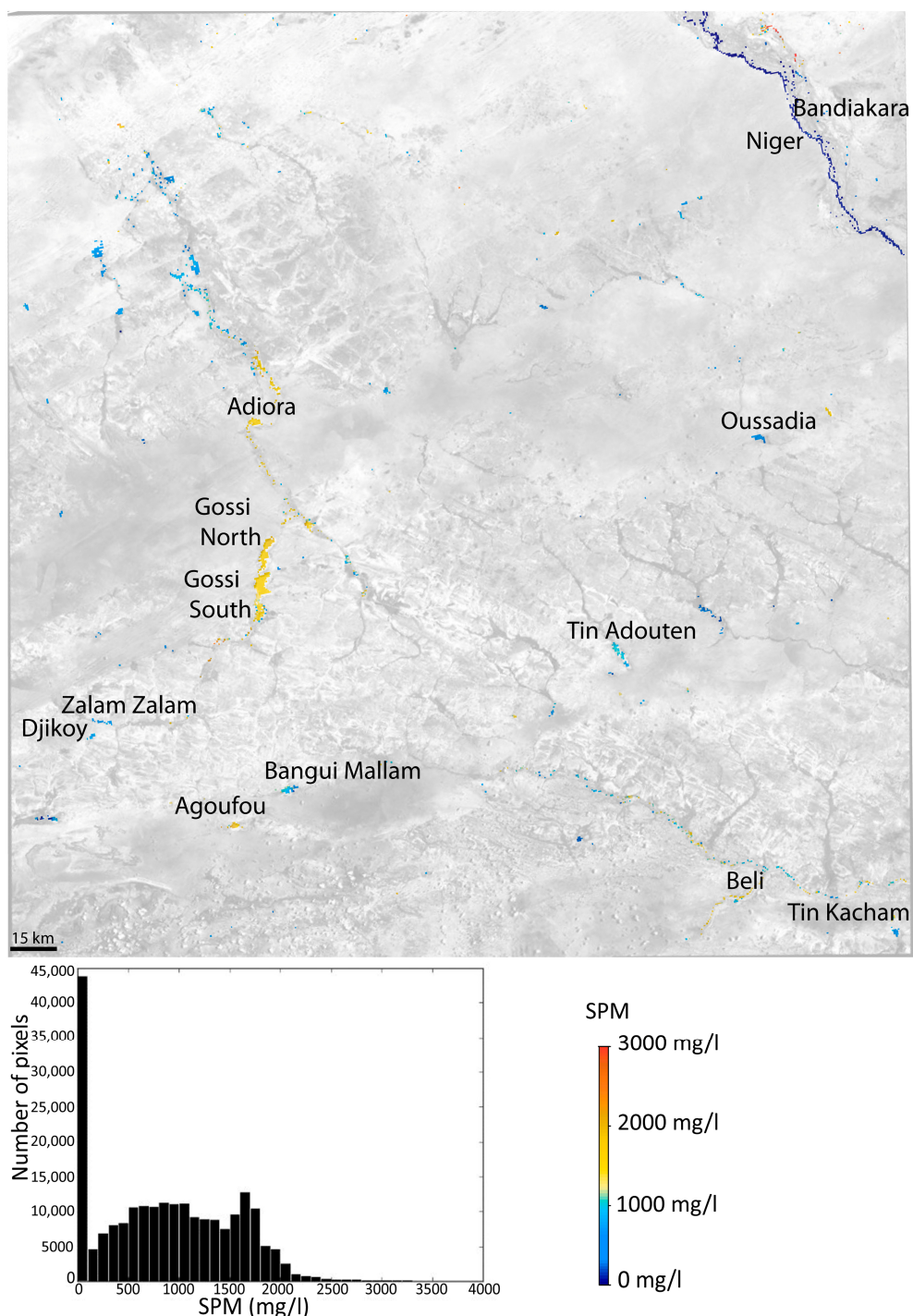


**Figure 14.** SPM values derived from the Landsat 8 image acquired on 24 August 2013 and histogram showing SPM values for all the pixels classified as water in the scene.

#### 4. Discussion

SPM measured in-situ correlates well with the NIR reflectance from MODIS and Landsat. This implies that the high and highly variable dust loading in the atmosphere and the varying water vapor content typical of the Sahelian climate are handled reasonably well by the atmospheric correction schemes employed for these sensors. However, the relationships between in-situ SPM and Landsat 7 were not as good as for Landsat 8 and MODIS. Landsat 7 reflectance values were found to be generally higher than those of the other two sensors. This can be explained by differences in the calibration

chains, in atmospheric corrections, and in wavelength and band width. Indeed, the NIR and Red bands for Landsat 8 and MODIS and the corresponding measured reflectance are closer to each other than to Landsat 7 (Table 1). In-situ measurements of reflectance carried out using a spectro-radiometer in Burkina Faso (Bagré Lake) revealed a similar difference between the NIR reflectance corresponding to the Landsat 8 or Landsat 7 spectral response [51].

The NIR band proved to be the most suitable for SPM retrieval up to high values. So far, few studies have addressed such high SPM values in inland water and some of our conclusions are consistent with previous work addressing highly turbid estuaries [52]. For inland water, an exception is the work by Wang et al. [31], who also used the NIR band to monitor SPM in the Yangtze River, with values ranging from 22 to 2160 mg/L. Our study confirms the relevance of the NIR band and extends its use for values up to 2500 mg/L, with Landsat and MODIS being used separately or in combination.

The SWIR (Short-Wavelength Infrared) band has been suggested in some studies to retrieve SPM in very turbid waters. Knaep et al. [53] proposed an algorithm based on the SWIR band at 1020  $\mu\text{m}$  (i.e., Sentinel-3) and 1240  $\mu\text{m}$  (MODIS, VIIRS—Visible Infrared Imaging Radiometer Suite) to derive SPM up to 1400 mg/L. In our study, adding the SWIR bands from Landsat 8 did not improve the SPM retrievals. This is probably due to the fact that Landsat 8 bands (band 6 at 1.56–1.66  $\mu\text{m}$  and band 7 at 2.1–2.3  $\mu\text{m}$ ) have higher wavelengths than those provided by Sentinel-3 and MODIS (the MODIS band at 1240  $\mu\text{m}$  couldn't be tested on the Agoufou Lake given its coarser spatial resolution).

Given the high values of SPM and turbidity, the fact that the water level of the Agoufou Lake remains higher than 1 m and the relationships between in-situ SPM and satellite reflectance also holds at the end of the dry season, when water levels are at a minimum, implies that background effects on the reflectance can be excluded. In addition, we found little evidence for edge effects (see Figures 12 and 13), which is probably due to the mask employed to define pure water pixels.

The seasonal SPM variability of the Agoufou Lake, and more generally of the lakes and ponds in this region, was found to be dependent on meteorological factors. First of all, the most significant increase in SPM is related to precipitation and occurs in the first half of the rainy season, which triggers large surface runoff, especially in areas where vegetation is not yet developed. Later in the rainy season, the development of the vegetation, as well as a possible limitation of available erodible material, reduces surface runoff and sediment transport. In the early dry season, when winds are usually moderate, SPM decreases due to particle deposition. A second important SPM peak is observed during the dry season in all but the driest years. This peak is linked to the resuspension of sediments caused by high winds during the Harmattan period, and possibly favored, for some lakes, by an important fetch since the surfaces of the lakes are still relatively large during this period. Wind-driven resuspension in shallow lakes has been reported in different areas [41], including the Sahel. Sané et al. [42] pointed out its impact for the Guiers Lake in Senegal, which is 2 m deep on average. The maximum depth for the Agoufou Lake and other lakes in the Gourma area is typically a few meters and the depth regularly decreases toward the shoreline. The final SPM decay, in the late dry season, is probably also linked to the wind regime and to the return of the monsoon flow. This period also corresponds to maximum downward radiation (shortwave plus longwave, Guichard et al. [44]), which possibly favors thermal stratification of the lake and would hinder resuspension.

Livestock numbers have not been found to be correlated with SPM. Surprisingly, the late season maximum in livestock numbers, caused by concentration around the few permanent water bodies, is a period of minimum SPM.

A significant increasing trend in SPM was observed for the Agoufou Lake using the whole MODIS time series. It corresponds to an increase in the NIR reflectance of 8%, which is higher than the calibration drift (less than 2%) identified for MODIS collection 6 [48]. The increasing SPM trend is consistent with the runoff increase observed in this area [7,36]. Our results suggest that both the extent in turbid water surface and SPM within these lakes may increase in parallel, due to changes in surface characteristics and/or to the intensification of rainfall events [8–10]. Moreover, an increasing trend of

SPM was also observed for the Bagré Lake in sub-humid West Africa (with a 19% increase between 2000 and 2015, Robert et al. [28]).

## 5. Conclusions

This study assessed the capability of high and medium resolution satellite sensors to monitor SPM in a Sahelian region. The important variability in the hydrological cycle at the seasonal and interannual time scale, the extremely high values of turbidity and SPM found in this region, and the strong and variable atmospheric load (aerosols and water vapor) were potentially challenging for a remote sensing approach. This study proved that NIR reflectance data from MODIS and Landsat are well suited to retrieve SPM values up to 2500 mg/L ( $R^2 = 0.79$ , bias = 20.3 mg/L, RMSE = 290 mg/L, %Diff = 3.8, %AbsDiff = 15.4) in this region, though there is room for algorithm improvement in atmospheric correction and SPM retrieval.

SPM derived from MODIS and Landsat were used to investigate the SPM spatio-temporal variability in Sahelian lakes and ponds and its drivers. We have found that SPM variability results from a combination of hydrological and atmospheric processes, resulting in a strong but complex seasonal cycle, a substantial inter annual variability, with particle resuspension occurring during most but not all years, usually high to very high SPM values, and a marked spatial variability.

Finally, a 27% increasing trend of SPM was observed for the Agoufou Lake over the 2000–2016 period. This could be due to either precipitation intensification [9], or an increase in erosion over the Agoufou watershed [7], or both. Poor water quality and related health hazards are among the possible consequences of increasing SPM in surface waters. Turbid water often carries microbiological contaminants, which combines with the health vulnerabilities of local populations to produce microbiological health risks. Since environmental monitoring infrastructures are presently scarce in the Sahel, satellite monitoring of small water bodies, made possible with the high resolution of Landsat and Sentinel-2 time series, opens important perspectives for understanding the physical mechanisms regulating the SPM spatio-temporal variability and for mapping water quality and related health hazards in this region.

**Acknowledgments:** This work has been supported by the French Programme National de Télédétection Spatiale (PNTS, <http://www.insu.cnrs.fr/pnts>), grant No. PNTS-2015-10 and the French Centre National d'Etudes Spatiales (CNES) through a grant to the first author. This research was based on data from the AMMA-CATCH observatory, whose coordinator of the Mali site is Eric Mougin. The authors thank Laetitia Gal and Pierre Hiernaux for their expertise on the hydrological system of the Agoufou Lake, Cindy Gosset for discussions on satellite data, and Ali Maiga and Hamma Maiga for the field measurements. We thank the anonymous reviewers and the editor for their useful comments on an earlier version of the manuscript.

**Author Contributions:** Elodie Robert, Laurent Kergoat, Manuela Grippa designed the study, performed the analyses and wrote the manuscript, Nogmana Soumaguel and Mamadou Diawara collected in situ data, Sébastien Merlet processed MODIS data, Jean-Michel Martinez contributed MODIS algorithms and granulometry data.

**Conflicts of Interest:** The authors declare no conflict of interest.

## References

1. Descroix, L.; Mahé, G.; Lebel, T.; Favreau, G.; Galle, S.; Gautier, E.; Olivry, J.; Albergel, J.; Amogu, O.; Cappelaere, B.; et al. Spatio-temporal variability of hydrological regimes around the boundaries between Sahelian and Sudanian areas of West Africa: A synthesis. *J. Hydrol.* **2009**, *375*, 1–2. [[CrossRef](#)]
2. Favreau, G.; Cappelaere, B.; Massuel, S.; Leblanc, M.; Boucher, M.; Boulain, N.; Leduc, C. Land clearing, climate variability, and water resources increase in semiarid southwest Niger: A review. *Water Resour. Res.* **2009**, *45*, 1–18. [[CrossRef](#)]
3. Leblanc, M.J.; Favreau, G.; Massuel, S.; Tweed, S.O.; Loireau, M.; Cappelaere, B. Land clearance and hydrological change in the Sahel: SW Niger. *Glob. Planet. Chang.* **2008**, *61*, 135–150. [[CrossRef](#)]
4. Gardelle, J.; Hiernaux, P.; Kergoat, L.; Grippa, M. Less rain, more water in ponds: A remote sensing study of the dynamics of surface waters from 1950 to present in pastoral Sahel (Gourma region, Mali). *Hydrol. Earth Syst. Sci.* **2010**, *14*, 309–324. [[CrossRef](#)]

5. Gal, L.; Grippa, M.; Hiernaux, P.; Peugeot, C.; Mougin, E.; Kergoat, L. Changes in lakes water volume and runoff over ungauged Sahelian watersheds. *J. Hydrol.* **2016**, *540*, 1176–1188. [[CrossRef](#)]
6. Dardel, C.; Kergoat, L.; Hiernaux, P.; Grippa, M.; Mougin, E.; Ciais, P.; Nguyen, C.-C. Rain-Use-Efficiency: What it Tells about the Conflicting Sahel Greening and Sahelian Paradox. *Remote Sens.* **2014**, *6*, 1–26. [[CrossRef](#)]
7. Gal, L.; Grippa, M.; Hiernaux, P.; Pons, L.; Kergoat, L. Modeling the paradoxical evolution of runoff in pastoral Sahel. The case of the Agoufou watershed, Mali. *Hydrol. Earth Syst. Sci.* **2017**, *21*, 4591–4613. [[CrossRef](#)]
8. Frappart, F.; Hiernaux, P.; Guichard, F.; Mougin, E.; Kergoat, L.; Arjounin, M.; Lavenu, F.; Koité, M.; Paturel, J.-E.; Lebel, T. Rainfall regime across the Sahel band in the Gourma region, Mali. *J. Hydrol.* **2009**, *375*, 128–142. [[CrossRef](#)]
9. Panthou, G.; Vischel, T.; Lebel, T. Recent trends in the regime of extreme rainfall in the Central Sahel. *Int. J. Climatol.* **2014**, *34*, 3998–4006. [[CrossRef](#)]
10. Taylor, C.; Belušić, D.; Guichard, F.; Parker, D.J.; Vischel, T.; Bock, O.; Harris, P.P.; Janicot, S.; Klein, C.; Panthou, G. Frequency of extreme Sahelian storms tripled since 1982 in satellite observations. *Nature* **2017**, *544*, 475–478. [[CrossRef](#)] [[PubMed](#)]
11. Rochelle-Newall, E.; Nguyen, T.M.H.; Le, T.P.Q.; Sengtaheuanghoun, O.; Riblozi, O. A short review of fecal indicator bacteria in tropical aquatic ecosystem: Knowledge gaps and future directions. *Front. Microbiol.* **2015**, *6*, 1–15. [[CrossRef](#)] [[PubMed](#)]
12. Troeger, C.; Forouzanfar, M.; Rao, P.C.; Khalil, I.; Brown, A.; Reiner, R.C.; Fullman, N., Jr.; Thompson, R.L.; Abajobir, A.; Ahmed, M.; et al. Estimates of global, regional, and national morbidity, mortality, and aetiologies of diarrhoeal diseases: A systematic analysis for the Global Burden of Disease Study 2015. *Lancet Infect. Dis.* **2017**. [[CrossRef](#)]
13. Gangneron, F.; Becerra, S.; Dia, A.H. Des pompes et des hommes. État des lieux des pompes à motricité humaine d'une commune du Gourma malien. *Autrepart* **2010**, *3*, 39–56. [[CrossRef](#)]
14. Gangneron, F.; Becerra, S.; Dia, A.H. L'étonnante diversité des ressources en eau à Hombori. Entre contrastes environnementaux, pratiques locales et technologies extérieures. *Revue Tiers Monde* **2010**, *4*, 109–128. [[CrossRef](#)]
15. Doxaran, D.; Ruddick, K.; McKee, D.; Gentili, B.; Tailliez, D.; Chami, M.; Babin, M. Spectral variations of light scattering by marine particles in coastal waters, from visible to near infrared. *Limnol. Oceanogr.* **2009**, *54*, 1257–1271. [[CrossRef](#)]
16. Petus, C.; Chust, G.; Gohin, F.; Doxaran, D.; Froidefond, J.M.; Sagarminaga, Y. Estimating turbidity and total suspended matter in the Adour River plume (South Bay of Biscay) using MODIS 250-m imagery. *Cont. Shelf Res.* **2010**, *30*, 379–392. [[CrossRef](#)]
17. Babin, M.; Morel, A.; Fournier-Sicre, V.; Fell, F.; Stramski, D. Light scattering properties of marine particles in coastal and open ocean waters as related to the particle mass concentration. *Limnol. Oceanogr.* **2003**, *48*, 843–859. [[CrossRef](#)]
18. Dogliotti, A.I.; Ruddick, K.G.; Nechad, B.; Doxaran, D.; Knaeps, E. A single algorithm to retrieve turbidity from remotely-sensed data in all coastal and estuarine waters. *Remote Sens. Environ.* **2015**, *156*, 157–168. [[CrossRef](#)]
19. Moore, G.K. Satellite remote sensing of water turbidity/Sonde de télémesure par satellite de la turbidité de l'eau. *Hydrol. Sci. Bull.* **1980**, *25*, 407–421. [[CrossRef](#)]
20. Morel, A.; Prieur, L. Analysis of variation in ocean color. *Limnol. Oceanogr.* **1977**, *22*, 709–722. [[CrossRef](#)]
21. Morel, A.; Gentili, B. Diffuse reflectance of oceanic waters. III. Implication of bidirectionality for the remote-sensing problem. *Appl. Opt.* **1996**, *35*, 4850–4862. [[CrossRef](#)] [[PubMed](#)]
22. Nechad, B.; Ruddick, K.G.; Park, Y. Calibration and validation of a generic multisensor algorithm for mapping of total suspended matter in turbid waters. *Remote Sens. Environ.* **2010**, *114*, 854–866. [[CrossRef](#)]
23. Novoa, S.; Doxaran, D.; Ody, A.; Vanhellemont, Q.; Lafon, V.; Lubac, B.; Gernez, P. Atmospheric corrections and multi-conditional algorithm for multi-sensor remote sensing of suspended particulate matter in low-to-high turbidity levels coastal waters. *Remote Sens.* **2017**, *9*, 61. [[CrossRef](#)]
24. Martinez, J.-M.; Guyot, J.-L.; Filizola, N.; Sondag, F. Increase in suspended sediment discharge of the Amazon River assessed by monitoring network and satellite data. *Catena* **2009**, *79*, 257–264. [[CrossRef](#)]

25. Martinez, J.-M.; Espinoza-Villar, R.; Armijos, E.; Silva Moreira, L. The optical properties of river and floodplain waters in the Amazon River Basin: Implications for satellite-based measurements of suspended particulate matter. *J. Geophys. Res.* **2015**, *120*, 1274–1287. [[CrossRef](#)]
26. Feng, L.; Hu, C.; Chen, X.; Tian, L.; Chen, L. Human induced turbidity changes in Poyang Lake between 2000 and 2010: Observations from MODIS. *J. Geophys. Res.* **2012**, *117*, 1–19. [[CrossRef](#)]
27. Kaba, E.; Philpot, W.; Steenhuis, T. Evaluating suitability of MODIS-Terra images for reproducing historic sediment concentrations in water bodies: Lake Tana, Ethiopia. *Int. J. Appl. Earth Obs. Geoinform.* **2014**, *26*, 286–297. [[CrossRef](#)]
28. Robert, E.; Grippa, M.; Kerfoot, L.; Pinet, S.; Gal, L.; Cochonneau, G.; Martinez, J.-M. Monitoring water turbidity and surface suspended sediment concentration of the Bagre Reservoir (Burkina Faso) using MODIS and field reflectance data. *Int. J. Appl. Earth Obs. Geoinform.* **2016**, *52*, 243–251. [[CrossRef](#)]
29. Janicot, S.; Ali, A.; Asencio, N.; Berry, G.; Bock, O.; Bourles, B.; Caniaux, G.; Chauvin, F.; Deme, A.; Kerfoot, L.; et al. Large-scale overview of the summer monsoon over West and Central Africa during the AMMA field experiment in 2006. *Ann. Geophys.* **2008**, *26*, 2569–2595. [[CrossRef](#)]
30. Gernez, P.; Lafon, V.; Lerouxel, A.; Curti, C.; Lubac, B.; Cerisier, S.; Barill, L. Toward sentinel-2 high resolution remote sensing of suspended particulate matter in very turbid waters: SPOT4 (Take5) experiment in the Loire and Gironde estuaries. *Remote Sens.* **2015**, *7*, 9507–9528. [[CrossRef](#)]
31. Wang, J.-J.; Lu, X.X.; Liew, S.C.; Zhou, Y. Retrieval of suspended sediment concentrations in large turbid rivers using Landsat ETM+: An example from the Yangtze River, China. *Earth Surface Process. Landf.* **2009**, *34*, 1082–1092. [[CrossRef](#)]
32. Soti, V.; Puech, C.; Lo Seen, D.; Bertran, A.; Vignolles, C.; Mondet, B.; Dessay, N.; Tran, A. The potential for remote sensing and hydrologic modelling to assess the spatio-temporal dynamics of ponds in the Ferlo Region (Senegal). *Hydrol. Earth Syst. Sci.* **2010**, *14*, 1449–1464. [[CrossRef](#)]
33. Haas, E.M.; Bartholomé, E.; Combal, B. Time series analysis of optical remote sensing data for the mapping of temporary surface water bodies in sub-Saharan western Africa. *J. Hydrol.* **2009**, *370*, 52–63. [[CrossRef](#)]
34. Mougin, E.; Hiernaux, P.; Kerfoot, L.; Grippa, M.; de Rosnay, P.; Timouk, F.; Le Dantec, V.; Demarez, V.; Lavenu, F.; Arjounin, M.; et al. The AMMA-CATCH Gourma observatory site in Mali: Relating climatic variations to changes in vegetation, surface hydrology, fluxes and natural resources. *J. Hydrol.* **2009**, *375*, 14–33. [[CrossRef](#)]
35. Lebel, T.; Cappelaere, B.; Galle, S.; Hanan, N.; Kerfoot, L.; Levis, S.; Vieux, B.; Descroix, L.; Gosset, M.; Mougin, E.; et al. AMMA-CATCH studies in the Sahelian region of West-Africa: An overview. *J. Hydrol.* **2009**, *375*, 1–2. [[CrossRef](#)]
36. Gal, L. Modélisation de l'évolution Paradoxe de l'hydrologie Sahélienne: Application au Bassin d'Agoufou (Mali). In *Interfaces Continentales, Environnement*; Université Paul Sabatier: Toulouse, France, 2016. Available online: <https://tel.archives-ouvertes.fr/tel-01484584v2/document> (accessed on 6 November 2017).
37. Diawara, M.O. Impact de la Variabilité Climatique au Nord Sahel (Gourma, Mali) sur la Dynamique des Ressources Pastorales, Conséquences sur les Productions Animales. Ph.D. Thesis, Université Toulouse 3, Toulouse, France, 2015.
38. Prévost, Y. Analyse spatiale de la pression animale comme facteur de désertification dans le nord du Sénégal. In *Apports de la Télédétection à la Lutte Contre La Sécheresse*; Compte-rendu Des Journées Scientifiques de Thies: Thies, Sénégal, 1989.
39. Rokni, K.; Ahmad, A.; Selamat, A.; Hazini, S. Water Feature Extraction and Change Detection Using Multitemporal Landsat Imagery. *Remote Sens.* **2014**, *6*, 4173–4189. [[CrossRef](#)]
40. Xu, H. Modification of normalised difference water index (NDWI) to enhance open water features in remotely sensed imagery. *Int. J. Remote Sens.* **2006**, *27*, 3025–3033. [[CrossRef](#)]
41. Carper, G.L.; Bachmann, R.W. Wind Resuspension of Sediments in a Prairie Lake. *J. Can. Sci. Halieut. Aquat.* **1984**, *41*, 1763–1767. [[CrossRef](#)]
42. Sané, S.; Ba, N.; Samb, P.I.; Noba, K.; Arfi, R. Moteurs et conséquences de la resuspension dans un lac sahélien peu profond: Le lac de Guiers au Sénégal. *Int. J. Biol. Chem. Sci.* **2015**, *9*, 927–943. [[CrossRef](#)]
43. Lövstedt, C.B.; Bengtsson, L. The role of non-prevailing wind direction on resuspension and redistribution of sediments in a shallow lake. *Aquat. Sci.* **2008**, *70*, 304–313. [[CrossRef](#)]

44. Guichard, F.; Kergoat, L.; Mougin, E.; Timouk, F.; Baup, F.; Hiernaux, P.; Lavenu, F. Surface thermodynamics and radiative budget in the Sahelian Gourma: Seasonal and diurnal cycles. *J. Hydrol.* **2009**, *375*, 161–177. [[CrossRef](#)]
45. Sterk, G. Causes, consequences and control of wind erosion in Sahelian Africa: A review. *Land. Degrad. Dev.* **2003**, *14*, 95–108. [[CrossRef](#)]
46. Green, M.O.; Coco, G. Review of wave-driven sediment resuspension and transport in estuaries. *Rev. Geophys.* **2014**, *52*, 77–117. [[CrossRef](#)]
47. Dardel, C.; Kergoat, L.; Hiernaux, P.; Mougin, E.; Grippa, M.; Tucker, C.J. Re-greening Sahel: 30 years of remote sensing data and field observations (Mali, Niger). *Remote Sens. Environ.* **2014**, *140*, 340–364. [[CrossRef](#)]
48. Doelling, D.R.; Wu, A.; Xiong, X.; Scarino, B.R.; Bhatt, R.; Haney, C.O.; Morstad, D.; Gopalan, A. The radiometric stability and scaling of collection 6 Terra-and Aqua-MODIS VIS, NIR, and SWIR spectral bands. *IEEE Trans. Geosci. Remote Sens.* **2015**, *53*, 4520–4535. [[CrossRef](#)]
49. Beuselinck, L.; Govers, G.; Steegen, A.; Hairsine, P.B.; Poesen, J. Evaluation of the simple settling theory for predicting sediment deposition by overland flow. *Earth Surface Process. Landf.* **1999**, *24*, 993–1007. [[CrossRef](#)]
50. Brune, G.M. Trap efficiency of reservoirs. *Trans. Am. Geophys. Union* **1953**, *34*, 407–418. [[CrossRef](#)]
51. Pinet, S.; Martinez, J.M.; Gosset, C.; Grippa, M.; Robert, E.; Ouillon, S.; Kergoat, L. Monitoring of suspended particulate matter concentration using sentinel-2, landsat-8 and spot-5 data over highly turbid waters in a West African reservoir. In preparation.
52. Doxaran, D.; Froidefond, J.M.; Lavender, S.; Castaing, P. Spectral signature of highly turbid waters: Application with SPOT data to quantify suspended particulate matter concentrations. *Remote Sens. Environ.* **2002**, *81*, 149–161. [[CrossRef](#)]
53. Knaeps, E.; Ruddick, K.G.; Doxaran, D.; Dogliotti, A.I.; Nechad, B.; Raymaekers, D.; Sterckx, S. A SWIR based algorithm to retrieve total suspended matter in extremely turbid waters. *Remote Sens. Environ.* **2015**, *168*, 66–79. [[CrossRef](#)]



© 2017 by the authors. Licensee MDPI, Basel, Switzerland. This article is an open access article distributed under the terms and conditions of the Creative Commons Attribution (CC BY) license (<http://creativecommons.org/licenses/by/4.0/>).